Comparison between low-order and high-order acoustic pressure solvers for bubbly media computations

G S Bruno Lebon[1], I Tzanakis[2], K A Pericleous[1] and D G Eskin[2]

[1] Centre for Numerical Modelling and Process Analysis, The University of Greenwich, London, SE10 9ET, United Kingdom
[2] Brunel Centre for Advanced Solidification Technology, Brunel University, Uxbridge, Middlesex, UB8 3PH, United Kingdom

E-mail: G.S.B.Lebon@gre.ac.uk

Abstract. Numerical modelling is a useful tool for the fundamental study of acoustic cavitation treatment in liquid metals. This treatment, also known as ultrasonic melt processing, significantly improves the properties and quality of metallic materials. However, the mechanisms leading to these observed improvements are still unclear and a fundamental study of cavitation treatment is required to understand this process. In this endeavour, this paper compares the use of high-order discretization schemes for solving acoustic pressures in cavitating liquids with its low-order counterpart. A fourth order scheme is shown to be more stable and accurate than a second order scheme when taking into account the acceleration of bubbles before their collapse, and is recommended for the full cavitation modelling of acoustic treatment of liquid metals.

1. Introduction

Ultrasonic treatment yields significant improvements in the quality and properties of metallic materials [1-3]. These improvements are attributed to acoustic cavitation [4]. However, this promising technology has not been successfully applied in the treatment of large volumes of melt, as is required by industrial processes like continuous casting. A fundamental study of the melt cavitation process is therefore required to circumvent difficulties in scaling up the ultrasonic treatment process [5]. The '*full cavitation model*' [6], originally developed for hydrodynamic cavitation in water, has been used by Nastac [7] and the present authors [10-11] to predict the cavitation treatment zone in a crucible and a launder respectively. Accurate prediction of these cavitation regions is required to optimize launder designs and minimize the power input, complexity, and time required to treat a certain volume of liquid metal. However, the pressure discretization models used so far [9-11] are at most second order in space and time, making the computations prone to numerical diffusion over long simulation run times. This paper investigates the use of higher-order methods in the discretization of the acoustic wave equations as applied to cases where the acoustic pressures are very large, to pave the way for longer simulations of ultrasonic melt treatment.

2. Theory

In the present model, the acoustic pressure p, acoustic wave velocities v_i, and bubble volume fraction ϕ are solved for in a segregated manner.

2.1. Governing equations

Conservation of mass and momentum, and the identity $\partial p/\partial \rho \equiv c^2$, where ρ is the medium's density, give the equations for the propagation of sound in a moving fluid medium:

$$\frac{\partial p}{\partial t} + \overline{v}_j \frac{\partial p}{\partial x_j} + \bar{p} c^2 \frac{\partial v_j}{\partial x_j} = S \tag{1}$$

$$\frac{\partial v_i}{\partial t} + \overline{v}_j \frac{\partial v_i}{\partial x_j} + \frac{1}{\bar{\rho}} \frac{\partial \mathrm{p}}{\partial x_i} = \frac{\partial \tau_{ij}}{\partial x_j} + F_i \tag{2}$$

S contains mass sources such as sinusoidal signals representing the vibrating surface of a sonotrode or the contribution of the growth and collapse of cavitation bubbles to the acoustic pressure ($-\rho c^2 \partial \phi / \partial t$). The forcing terms F_i contain velocity sources due to the vibrating surface. The material properties symbols are described in Table 1 and the overbar indicates mean flow variables. The speed of sound c in the bubbly fluid is variable and depends on the resonant frequency of the oscillating bubbles. For frequencies much lower than the resonant frequency of the bubbles present in the liquid, $c = \sqrt{\frac{K_b K_l}{\{\phi K_l + (1-\phi) K_b\}[\phi \overline{\rho_b} + (1-\phi)\overline{\rho_l}]}}$ where K represents the bulk modulus of the phase and the subscripts b and l denote bubble and liquid properties respectively [10]. The governing equation for the bubble volume fraction ϕ is

$$\frac{\partial (\overline{\rho_b} \phi)}{\partial t} + \frac{\partial (\overline{\rho_b v_j} \phi)}{\partial x_j} = \Gamma \tag{3}$$

where Γ is the net phase change. Following the derivation of the full cavitation model [6], by using the Keller-Miksis equation – which is numerically stable for the large forcing amplitudes that are encountered in ultrasonic melt treatment [11] – and keeping the acceleration term [12], the net phase change rate for bubble growth is obtained as

$$\Gamma = C_g \frac{v_{ch}}{\sigma} \rho_l \rho_b \left[\frac{2}{3} \left(\frac{1 + v_{ch}/c}{1 - v_{ch}/3c} \right) \frac{p_v - P}{\rho_l} - \frac{2}{3} R \frac{d^2 R}{dt^2} \right]^{1/2} (1 - \phi) \tag{4}$$

applicable for $p_v > P$. For the collapse phase, i.e. $P > p_v$, the phase change rate is

$$\Gamma = -C_c \frac{v_{ch}}{\sigma} \rho_l \rho_b \left[\frac{2}{3} \left(\frac{1 + \frac{v_{ch}}{c}}{1 - \frac{v_{ch}}{3c}} \right) \frac{P - p_v}{\rho_l} - \frac{2}{3} R \frac{d^2 R}{dt^2} \right]^{\frac{1}{2}} \phi \tag{5}$$

v_{ch} is a characteristic bubble velocity that is estimated from an average bubble size [9], and C_g and C_c are empirical coefficients.

2.2. Wave equations discretization

A fully staggered mesh is used in both differencing schemes presented: the scalar quantities acoustic pressure and bubble volume fraction are stored in cell centres at the end of each time step, and velocity components are stored at cell faces in the middle of each time step [13].

2.2.1. Leapfrog scheme. The leapfrog scheme is second order in space and time. The acoustic pressures and velocities are updated using the following relations:

$$p^k = p^{k-1} - \frac{\mathrm{c}\Delta \mathrm{t}}{\mathrm{x_i}} \left(u_{i,dwnd}^{k-\frac{1}{2}} - u_{i,upwnd}^{k-\frac{1}{2}} \right) + \mathrm{S}\Delta \mathrm{t} \tag{6}$$

$$u_i^{k+\frac{1}{2}} = u_i^{k-\frac{1}{2}} - \mathrm{c}\Delta \mathrm{t} \left(p_{dwnd}^k - p_{upwnd}^k \right) + \mathrm{F_i}\Delta \mathrm{t} \tag{7}$$

2.2.2. Fourth-order scheme. The dispersion-relation-preserving scheme [14] is used for the spatial differentiation and temporal integration steps of the convective terms in equations (1) and (2).

The 6-point stencil for spatial derivatives is given by

$$\frac{df}{dx} = \frac{1}{\Delta x}\sum_{j=-2}^{3} a_j f\left[x + \left(j - \frac{1}{2}\right)\Delta x\right] \tag{8}$$

The temporal integration is given by

$$\int_{-\frac{\Delta T}{2}}^{\frac{\Delta T}{2}} f(t)dt = \Delta t \sum_{m=0}^{3} b_m f(-m\Delta t) \tag{9}$$

with the coefficients a_j and b_m calculated so that the spatial and temporal schemes are fourth-order and third-order accurate respectively [13].

3. Problem description

For the example case presented in this paper, the geometry is the rectangular cuvette used by Žnidarčič *et al* [12]: the base is a 25 mm x 25 mm square, and liquid water with material properties given in Table 1 is filled up to a height of 50 mm. A 3 mm diameter sonotrode is immersed in the liquid at the axis of the cuvette, with the vibrating surface resting at 30 mm from the bottom. The sonotrode vibrates with an amplitude of 164 μm and frequency 20 kHz, with a power input Q_{us} of 70 W. The resulting acoustic pressure is calculated as $p_{max} = \sqrt{2\rho c\, {Q_{us}}/{A}}$, where A is the surface area of the sonotrode [15].

Table 1: Material properties of aluminium and water [1]. Surface tension with hydrogen interface for aluminium and air interface for water.

Material Property	Aluminium (700 ºC)	Water (20 ºC)
Sound speed c (m s^{-1})	4600.	1482.
Density ρ_l (kg m^{-3})	2375.	1000.
Dynamic viscosity μ_l (mPa s)	1.0	1.004
Surface tension σ (N m^{-1})	0.860	0.079
Vapour pressure p_v (kPa)	Negligible	2.2
Bulk modulus K (GPa)	41.2	2.15

4. Results and conclusions

Figure 1 shows the computed acoustic pressure at a probe position that is 7 mm horizontally from the vibrating surface of the sonotrode using the fourth-order solver. Figure 2 shows the predicted pressure profile in the cuvette. Three cases were run: with the fourth-order solver including the acceleration term in source terms (4) and (5), the fourth-order solver without the acceleration term, and the second order solver without the acceleration term. The same Courant number of 0.2 and a grid size of 0.5 mm were used. The fourth-order scheme converges with the acceleration term included while the second-order leapfrog scheme diverges. The second-order scheme converges to a wrong solution without the acceleration term. This instability arises in the second-order scheme because of the inaccurate prediction of acoustic pressure, which then results in an inaccurate bubble distribution profile: this is fed back to the pressure solver in the next iteration.

The fourth-order scheme is therefore more suitable for handling large acoustic pressures and bubble fraction variations; the higher-order method is both less prone to numerical diffusion and accurate with large Courant numbers of order 0.2. Since ultrasonic melt treatment processes are long – melt treatment in a typical crucible is of the order of minutes –, the numerical scheme for modelling acoustic cavitation will always suffer from numerical diffusion creeping in as the solution advances in time. Higher-order methods are therefore required in these cases so that numerical simulations can run to completion, without unrealistic prediction of acoustic pressures.

However, the method does not resolve the peaks arising from bubble collapses accurately: this is an inherent property of the homogeneous model. The fine details of the bubble dynamics are sacrificed to recover their overall effect on the domain acoustic pressure. This is to enable a sufficiently accurate simulation involving large time steps, which is a requirement for industrial-scale design of experiments simulations. This feature is crucial for the optimization of launder and crucible flow configurations, as would be required by industrial processes involving ultrasonic melt treatment. A numerical simulation employing baffles to increase the treatment time of liquid metal in cavitation zones will benefit from a higher-order scheme for the solution of acoustic pressure.

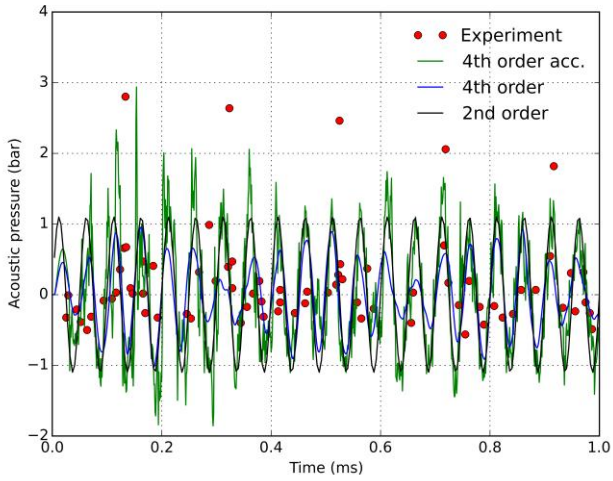

Figure 1: Comparison between predicted acoustic pressure at probe position for different solvers and experimental data from [12].

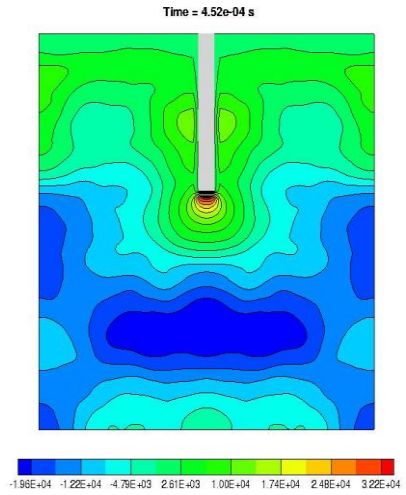

Figure 2: Computed acoustic pressure contour with the fourth-order spatial scheme.

Acknowledgements
The authors are grateful to the UK Engineering and Physical Sciences Research Council (EPSRC) for financial assistance for this research in contract numbers: EP/K00588X/1 and EP/K005804/1.

References
[1] Eskin G I and Eskin D G 2014 *Ultrasonic Treatment of Light Alloy Melts* (CRC Press)
[2] Campbell J 1981 *Int. Mater. Rev.* **26** 71
[3] Cao G *et al* 2008 *Mater. Sci. Eng. A-Struct.* **486** 357
[4] Eskin G I 1995 *Ultrason. Sonochem.* **2** 137
[5] Komarov *et al* 2013 *Ultrason. Sonochem.* **20** 754
[6] Singhal A K *et al* 2002 *J. Fluid Eng.* **124** 617
[7] Nastac L 2011 *Metall. Mater. Trans. B* **42** 1297
[8] Lebon G S B *et al* 2015 *IOP Conf. Ser.: Mater. Sci. Eng.* **72** 052050
[9] Lebon G S B *et al* 2015 *Proc. 144th TMS Annual Meeting & Exhibition (Orlando) Advances in the Science and Engineering of Casting Solidification* p 23
[10] Cheeke J D N 2012 *Fundamentals and applications of ultrasonic waves* (CRC Press)
[11] Keller J B and Miksis M 1980 *J. Acoust. Soc. Am.* **68** 628
[12] Žnidarčič A *et al* 2014 *Ultrason. Sonochem.* **22** 482
[13] Djambazov *et al* 2000 *AIAA Journal* **38** 16
[14] Tam C K W and Webb J C 1993 *J. Comput. Phys.* **107** 262
[15] Van Iersel *et al* 2008 *Ultrason. Sonochem.* **15** 294